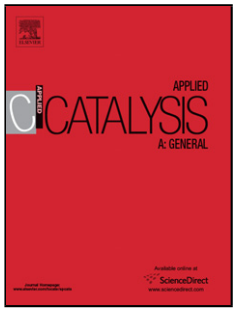

Title: Pd nanoparticles supported on 1H-benzotriazole functionalized carbon with enhanced catalytic performance towards ethanol oxidation

Author: Yanqin Liu Wei Wang Yan Yang Fengxia Wang Xiaolong Zhao Ziqiang Lei

PII: S0926-860X(15)30103-4
DOI: http://dx.doi.org/doi:10.1016/j.apcata.2015.08.008
Reference: APCATA 15502

To appear in: *Applied Catalysis A: General*

Received date: 23-4-2015
Revised date: 16-7-2015
Accepted date: 5-8-2015

Please cite this article as: Yanqin Liu, Wei Wang, Yan Yang, Fengxia Wang, Xiaolong Zhao, Ziqiang Lei, Pd nanoparticles supported on 1H-benzotriazole functionalized carbon with enhanced catalytic performance towards ethanol oxidation, Applied Catalysis A, General http://dx.doi.org/10.1016/j.apcata.2015.08.008

Pd nanoparticles supported on 1H-benzotriazole functionalized carbon with enhanced catalytic performance towards ethanol oxidation

Yanqin Liu [1], Wei Wang [2,*], Yan Yang [1], Fengxia Wang [1], Xiaolong Zhao [1], Ziqiang Lei [1,*]

1 Key Laboratory of Eco-Environment-Related Polymer Materials, Ministry of Education of China, Key Laboratory of Gansu Polymer Materials, College of Chemistry and Chemical Engineering, Northwest Normal University, Lanzhou 730070

2 School of Chemical and Biological Engineering, Lanzhou Jiaotong University, Lanzhou 730070

Graphical abstract

Abstract: Nitrogen functionalized carbon has received widely research interest because of their remarkable performance. In this paper, 1H-benzotriazole functionalized carbon (BTA-C) is fabricated and used as support to immobilize Pd nanoparticles. The physical characterization results demonstrate that the Pd nanoparticles uniformly disperse on the BTA-C. Because of the good effect of BTA functionalization, the as-prepared Pd/BTA-C catalyst has larger electrochemically active surface area contrasted to Pd/C. Meanwhile, the electrochemical test results indicate that the Pd/BTA-C possesses high activity (more than 1.8 times), lower onset potential

* Corresponding author, e-mail: wangwchem@163.com, Tel./Fax: +86 931 4938755.

* Corresponding author, e-mail: leizq@nwnu.edu.cn, leizq@hotmail.com, Tel./Fax: +86 931 7970261.

(negative 90 mV) and better stability than that of Pd/C counterpart in ethanol oxidation reaction. All results imply that the Pd/BTA-C is a promising candidate electrocatalyst in direct ethanol fuel cells.

Key words: Pd nanoparticles; 1H-benzotriazole; Nitrogen-functionalized-carbon; Ethanol oxidation

1. Introduction

Recently, direct ethanol fuel cells (DEFCs) have received increasing interest as a promising energy source due to low toxicity, low membrane permeability and high energy density [1-3]. However, the electrocatalyst seriously hinders the commercialization of DEFCs. Although Pt-based catalyst is recognized as the best catalyst [4], its application is limited by easy poisoning, high cost and low abundance of Pt [5-7]. Therefore, Pd-based catalysts seem to be more promising [8-12].

The supports would influence the size and dispersion of Pd, which further affect catalytic property [13]. Carbon black is the most commonly used electrocatalyst support [14-15]. Nonetheless, the dissolution and aggregation of metal nanoparticles on carbon could lead to obvious activity loss [16]. Therefore, alternative supports are highly desirable [17].

Surface functionalization with selected molecular is an effective approach to manipulate and optimize the performance of carbon supports. More and more attentions are focused on the nitrogen functionalization because nitrogen has a comparable atomic size and five valence electrons for bonding with carbon atoms [18]. Nitrogen functionalization can modify interfacial and electronic properties of

carbon materials [15, 19]. It could also improve the dispersion of catalyst particle, decrease the particle size and enhance intrinsic catalytic activity [20]. More importantly, nitrogen-containing carbon has high surface nucleation sites that allows it can serve as active sites for anchoring metal particles, strengthening the metal-support interaction and leading to a high stability [21]. Recently, D-glucosamine hydrochloride, dimethyldiallylammonium chloride, polyvinylpyrrolidone, polyaniline et.al [11, 22-25], have been used to introduce the nitrogen-groups on the carbon materials, which immobilize Pd nanoparticles in electrocatalysts. Accordingly, they exhibit excellent activity and stability in ethanol oxidation reaction (EOR).

1H-Benzotriazole (BTA) is a bifunctional molecule with a phenyl group and an amino functional group, which could strongly interact with the carbon material. However, as a commonly nitrogenous substance, the BTA is rarely reported to prepare nitrogen-containing carbon and further loads noble metal nanoparticles. In this study, carbon black is functionalized using BTA in solvent at room temperature and further loads Pd nanoparticle (Pd/BTA-C) used as catalyst for EOR. The large electrochemically active surface area, low onset potential, high electrocatalytic activity and stability imply that Pd/BTA-C is a promising candidate electrocatalyst in DEFCs. The simplicity and effectiveness of BTA-C could also be applied for preparing other high-performance electrocatalysts.

2. Experimental

2.1 Preparation of catalyst

2.1.1 Synthesis of BTA-C support

1H-Benzotriazole (0.1 g) was dissolved in 50 ml ethanol. Then the pretreated carbon black (0.5 g) was added and dispersed using an ultrasonic bath, stirred for 18 h. Then Rotary Evaporator (RE-2000B) was used to dislodged the ethanol and the remained solid was dried at 50 ℃ for 7 h. Finally, the novel support was obtained, which is named as BTA-C.

2.1.2 Preparation of catalyst

$PdCl_2$ (41.7 mg) was dissolved with hydrochloric acid in 100 ml flask. Then 30 ml ethylene glycol (EG) and sodium citrate (150.0 mg) were added and stirred for l h. After the pH value of the solution was adjusted to ~8 by adding 5 wt % KOH / EG solution, the BTA-C (100.0 mg) was added to the flask with stirring and dispersing in an ultrasonic bath for 0.5 h, respectively. Following, the suspension was heated at 160 ℃ for 6 h under nitrogen protection. Then it was centrifuged, filtrated and dried at 50 ℃ for 12 h. Finally, the Pd (20 wt %)/BTA-C catalyst was obtained. The similar method was used to synthesize Pd (20 wt %)/C as a reference.

2.2 Characterization of catalysts and catalytic tests

The crystallinity of catalysts was characterized by X-ray diffraction (XRD). It was recorded on a Rigaku D/Max-2400 (Japan) diffractometer, using Cu K_a radiation operated at 40 kV and 150 mA. The morphology and structure of samples were examined by Transmission electron microscopy (TEM). They were performed on an Electron Microscope (Tecnai G^2 F20 S-TWIN TMP America). The surface compositions and states of elements were determined by X-ray photoelectron spectroscopy (XPS). It was carried out on an X-ray photoelectron spectrometer (Thi-

5702 America) with a monochromatic Al K_α X-ray source ($h\nu$ = 29.35 eV).

An Autolab electrochemical work station (PGSTAT128N, Eco Chemie, Netherlands) was used to perform the electrochemical experiments, including cyclic voltammetry, chronoamperometric response and linear sweep voltammetry. A conventional three-electrode cell was used, including an Ag/AgCl electrode as a reference, a platinum wire as a counter and a modified glassy carbon (5 mm in diameter) as a working electrode. The working electrode was prepared as follows: 5 mg catalyst was dispersed in 1 ml Nafion / Ethanol (0.25 % Nafion). 8 μl suspensions were quantitatively transferred to the surface of polished glassy carbon electrode. Before each measurement, the solution was purged with high-purity nitrogen gas for at least 10 min to ensure the gas saturated. In this study, the current was all normalized to Pd mass.

3. Results and discussion

3.1 Physical characterization

The crystal structure of as-prepared Pd/C and Pd/BTA-C was characterized by XRD. As displayed in Fig. 1, the broad peaks at about 22.5° can be indexed to the (002) reflection of carbon support. Meanwhile, the diffraction peaks at 40.0°, 46.4°, 68.0°, 82.0° and 86.4° correspond to the (111), (200), (220), (311) and (222) planes of the face-centered cubic (*fcc*) structure of Pd, respectively. Obviously, these peaks for Pd/C and Pd/BTA-C have no much difference. It implies that nitrogen functional groups on carbon support has no influence on the crystal structure of Pd.

XPS is a powerful tool to identify the elements' states. Fig. 2(a) shows the XPS spectrum of Pd/BTA-C. From the curve, distinct C 1s, N 1s, O 1s and Pd 3d signals can be recognized. The N 1s spectrum (Fig. 2(b)) around 400 eV can be de-convoluted into four peaks. It represents four types of bonding configurations of nitrogen within carbon structures: pyridinic-N (398.7 eV), pyrrolic-N (400.4 eV), graphitic-N (401.2 eV) and N-oxides of pyridinic-N (402.8 eV). The proportional amounts of pyridinic-N, pyrrolic-N, graphitic-N and N-oxides of pyridinic-N estimated by the peak were 2.0 %, 72.5 %, 21.9 % and 3.6 %, respectively.

The XPS spectra of C 1s ranging from 280.0 eV to 295.0 eV reveal the formation of various surface groups on the Pd/C (Fig. 3(a)) and Pd/BTA-C (Fig. 3(b)). The spectra could be deconvoluted into four components: C-C at 284.8 eV (labeled as C1), C-OH at 285.9 eV (labeled as C2), C-N at 287.1 eV (labeled as C3) and C-C=O (labeled as C4) at 289.0 eV. As can be seen from Tab. 1, the amount of C-N groups is increased on the carbon after BTA functionlization. Additionally, the decreased amounts of C-C and increased C-OH imply that functionalization not only introduces BTA on carbon but also increases the functional oxygen groups [26].

As shown in Fig. 3(c) and 3(d), the Pd in catalysts is composed of various chemical states. The Pd $3d_{5/2}$ spectrum is fitted with four symmetrical peaks around 335.4 eV (assigned to Pd^0), 336.2 eV (assigned to $Pd(OH)_x$)), 337.2 eV (assigned to PdO) and 338.0 eV (assigned to PdO_2) [27]. The results of the XPS

analysis are summarized in Tab. 2. Compared to Pd/C, the Pd/BTA-C sample shows a slightly higher level of Pd^0. This finding is consistent with literature [27] and would lead to enhanced catalytic properties for the EOR.

The morphology of the as-prepared catalysts was characterized by TEM. Fig. 4 displays the typical TEM images of the Pd/C and Pd/BTA-C. Obviously, the black is the Pd nanoparticles and the gray area is carbon support. It can be seen that the Pd nanoparticles are uniformly dispersed on BTA-C (Fig. 4(b)). While on carbon (Fig. 4(a)), some agglomeration are observed. The selected area electron diffraction (SAED) patterns (inserted) identify that two catalysts are polycrystalline structure [28]. The distribution histograms of Pd nanoparticles in Pd/C (Fig. 4(c)) and Pd/BTA-C (Fig. 4(d)) were obtained by measuring about 100 randomly selected particles. The mean size of Pd for Pd/C and Pd/BTA-C is 9.4 $\pm$ 0.6 nm and 7.8 $\pm$ 0.4 nm, respectively. Apparently, the results reveal that the BTA-C is more capable of forming well-dispersed metal particle [29], which would be beneficial to EOR. Fig. 4(e) and 4(f) show high-resolution TEM images of Pd/C and Pd/BTA-C catalysts. Obviously, both of them have good crystalline structures with the continuous ordered lattice fringes. The lattice spacing is 0.22 nm for Pd/C and Pd/BTA-C, respectively, which corresponds to the distance of the (111) crystal plane of the Pd (*fcc*).

3.2 Electrochemical measurements

The cyclic voltammetry of Pd/BTA-C was preliminarily investigated in 0.1 M KOH solution at a scan rate of 50 mV s^{-1}. As shown in Fig. 5(a), the oxidation peak

potential of Pd/BTA-C is about -0.56 V (*vs.* Ag/AgCl) and a broad reduction peak is around -0.27 V (*vs.* Ag/AgCl). Meanwhile, the peaks appear at -0.48 V and -0.25 V (*vs.* Ag/AgCl) for Pd/C, respectively. The difference of peaks may be attributed to the different supports.

As the activity of a catalyst is not only controlled by the catalytic properties but also by the surface area [30]. The electrochemically active surface area (EASA) has also been measured by determining the columbic charge for the reduction of palladium oxide. The EASA was calculated by using the equation follows [31]:

$$EASA = Q / SI$$

Q is the columbic charge;

S is a constant (0.405 mC cm^{-2});

I is the catalyst loading of Pd.

The EASA are accounted to be 312.8 cm^2 mg^{-1}_{Pd} and 583.0 cm^2 mg^{-1}_{Pd} for Pd/C and Pd/BTA-C, respectively. High EASA of Pd/BTA-C originates from the good dispersion of Pd nanoparticles and small Pd particle size, as well as probably a good conductivity of the BTA-C [12].

To further confirm the high catalytic activity of Pd/BTA-C, Fig. 5(b) shows the EOR results. There are two well-defined current peaks in catalysts. The anodic peak during the forward scan is caused by the electrocatalytic oxidation of ethanol. The current density of Pd/BTA-C (0.18 A mg^{-1}_{Pd}) is almost 1.8 times higher than that of Pd/C (0.10 A mg^{-1}_{Pd}). During the backward scan, the Pd oxides commence to be reduced at -0.25 V (*vs.* Ag/AgCl), which is attributed to the removal of reaction

intermediates [32]. The higher electrocatalytic activity for EOR on Pd/BTA-C than that of Pd/C shows Pd has a larger utilization in BTA-C, in agreement with the TEM results. Moreover, the onset potential of Pd/BTA-C (-0.61 V *vs.* Ag/AgCl) is remarkably lower than that of Pd/C (-0.52 V *vs.* Ag/AgCl). These indicate that the functionalization of BTA on carbon enhances electrocatalytic capability compared to Pd/C. Tab. 3 compares the performance of Pd/BTA-C with other nitrogen-containing carbon supported Pd catalyst towards EOR.

The electrochemical stability of these catalysts for EOR was then investigated by chronoamperometric experiments at -0.2 V (*vs.* Ag/AgCl). As shown in Fig. 5(c), it shows a gradual decrease in the oxidation current density with time in catalysts. The Pd/BTA-C exhibits a slower current decay over entire time scale in comparison with Pd/C. It proves a high tolerance to the carbonaceous species generated during EOR. Values after 3000 s, as shown in Fig. 5(d), are 0.020 A mg^{-1}_{Pd} and 0.026 A mg^{-1}_{Pd} on Pd/C and Pd/BTA-C, respectively. These indicate that the Pd/BTA-C catalyst is much more poisoning tolerant than Pd/C [33].

Fig. 6(a) shows a typical linear sweep voltammogram in 0.1 M KOH + 0.5 M C_2H_5OH solution. To reduce the mass transfer effect and derive kinetic parameters as much as possible, the scan rate is 1 mV s^{-1}, which is close to a steady-state polarization curve of the EOR on the Pd electrode [34-35]. Apparently, the oxidation current on the Pd/BTA-C is much larger than Pd/C. The corresponded Tafel plots ranged from -0.42 V to -0.12 V (*vs.* Ag/AgCl) are displayed in Fig. 6(b). Each plot could be fitted and divided into two linear regions according to the respective Tafel

196 slope. The values are 233.2 mV dec^{-1} *vs.* 204.2 mV dec^{-1} in low potential ranges and
197 409.7 mV dec^{-1} *vs.* 400.6 mV dec^{-1} in high potential ranges for Pd/C and Pd/BTA-C,
198 respectively. The Tafel slopes suggest the similar reaction mechanism and rate
199 determining step for the EOR at these potential ranges. Similar to methanol, the first
200 step of the EOR is the cleavage of O-H bond, forming ethoxy species CH_3CH_2O.
201 Further transformation of ethoxy species gives acetaldehyde CH_3CHO which then can
202 be oxidized by numerous reactions, forming several kinds of carbon oxides, such as
203 acetate ion, acetone, crotonaldehyde, other hydrocarbons, carbonate ion, carbon
204 monoxide, carbon dioxide and so on. These intermediates are adsorbed on the surface
205 of catalyst at lower potentials and the EOR could proceed when Pd-OH is generated
206 on the catalyst surface by dissociative adsorption of H_2O [36-38].

207 All of the above data reveal that the Pd/BTA-C exhibits enhanced catalytic
208 activity for EOR. It is worthwhile to say that high activity in electrochemical
209 performance observed here can probably be attributed to the BTA-C. The BTA is a
210 bifunctional molecule with a phenyl group and an amino functional group.
211 Introduction of nitrogen contained in BTA on carbon allows strong immobilization of
212 Pd nanoparticles due to strong cordination interactions between Pd and nitrogen [39],
213 leading to good dispersion and small size of Pd nanoparticles. It could provide more
214 active sites for EOR and increase the utilization of Pd. In addition, the long pair
215 electrons in nitrogen atoms increases the electronic conductivity of carbon substrate
216 [40]. Meanwhile, the nitrogen could influence the spin density and charge distribution
217 of the neighboring carbon atoms. This charge localization is conducive to help

participate in catalytic reactions directly [15]. Therefore, the Pd/BTA-C has high stability and enhanced activity for EOR.

4. Conclusion

In summary, 1H-benzotriazole functionalized carbon was prepared and used as support for Pd nanoparticles. The Pd nanoparticles are uniformly dispersed on BTA-C with small particle size. The Pd/BTA-C catalyst has larger EASA, lower onset potential, higher electrocatalytic activity and stability for EOR than that of Pd/C counterpart. It might be attributed to the high utilization of Pd nanoparticles on the BTA-C. Thus, the Pd/BTA-C is a promising candidate electrocatalyst in DEFCs.

Acknowledgement

We thank to the National Natural Science Foundation of China (21174114), the program for Changjiang Scholars and Innovative Research Team in University (IRT1177) and Innovative Research Team of Gansu Province (1210RJIA004).

References

[1] S.T. Nguyen, H.M. Law, H.T. Nguyen, N. Kristian, S. Wang, S.H. Chan, X Wang, Appl. Catal. B-Environ. 91 (2009) 507-515.

[2] S.S. John, P. Boolchand, A.P. Angelopoulos, Langmuir 29 (2013) 16150-16159.

[3] S.Q. Song, P. Tsiakaras, Appl. Catal. B-Environ. 63 (2006) 187-193.

[4] S.Q. Song, Y.R. Liang, Z.H. Li, Y. Wang, R.W. Fu, D.C. Wu, P. Tsiakaras, Appl. Catal. B-Environ. 98 (2010) 132-137.

[5] M.S. Ahmed, S. Jeon, ACS Catal. 4 (2014) 1830-1837.

[6] T. Arikan, A.M. Kannan, F. Kadirgan, Int. J. Hydrogen Energy 38 (2013) 2900-2907.

[7] F. Kadirgan, A.M. Kannan, T. Atilan, S. Beyhan, S.S. Ozenler, S. Suzer, A. Yörür, Int. J. Hydrogen Energy 34 (2009) 9450-9460.

[8] X.H. Xia, S.I. Choi, J.A. Herron, N. Lu, J. Scaranto, H.C. Peng, J. Wang, M. Mavrikakis, M.J. Kim, Y. Xia, J. Am. Chem. Soc. 135 (2013) 15706-15709.

[9] Z.L. Wang, J.M. Yan, H.L. Wang, Y. Ping, Q. Jiang, J. Mater. Chem. A 1 (2013) 12721-12725.

[10] C.W. Xu, H. Wang, P.K. Shen, S.P. Jiang, Adv. Mater. 19 (2007) 4256-4259.

[11] H.Y. Jin, T.Y. Xiong, Y. Li, X. Xu, M.M. Li, Y. Wang, Chem. Commun. 50 (2014) 12637-12640.

[12] G.Z. Hu, F. Nitze, T. Sharifi, H.R. Barzegar, T. Wågberg, J. Mater. Chem. A 22 (2012) 8541-8548.

[13] T. Maiyalagan, X. Wang, A. Manthiram, RSC. Adv. 4 (2014) 4028-4033.

[14] X. Xu, Y. Li, Y.T. Gong, P.F. Zhang, H.R. Li, Y. Wang, J. Am. Chem. Soc. 134 (2012) 16987-16990.

[15] K.N. Wood, R. O'Hayre, S. Pylypenko, Energy Environ. Sci. 7 (2014) 1212-1249.

[16] M.M. Liu, R.Z. Zhang, W. Chen, Chem. Rev. 114 (2014) 5117-5160.

[17] T.Z. Huang, S. Mao, H.H. Pu, Z.H. Wen, X.K. Huang, S.Q. Ci, J. Chen, J. Mater. Chem. A 1 (2013) 13404-13410.

[18] Y. L, Y. Z, H.H. C, Y. H, G.Q. S, L.M. D, L.T. Q, J. Am. Chem. Soc. 134

(2012) 15−18.

[19] F. Nitze, E. Abou-Hamad, T. Wågberg, Carbon 49 (2011) 1101-1107.

[20] Y.K. Zhou, K. Neyerlin, T.S. Olson, S. Pylypenko, J. Bult, H.N. Dinh, T. Gennett, Z. Shao, R. O'Hayre, Energy Environ. Sci. 3 (2010) 1437-1446.

[21] R.T. Lv, T.X. Cui, M.S. Jun, Q. Zhang, A. Cao, D.S. Su, Z. Zhang, S.H. Yoon, J. Miyawaki, I. Mochida, F. Kang, Adv. Funct. Mater. 21 (2011) 999-1006.

[22] M.M. Zhang, J.M. Xie, Q. Sun, Z.X. Yan, M. Chen, J.J. Jing, A.M. Showkot Hossain, Electrochim. Acta 111 (2013) 855-861.

[23] Y.T. Zhang, H.H. Shu, G. Chang, K. Ji, M. Oyama, X. Liu, Y.B. He, Electrochim. Acta 109 (2013) 570-576.

[24] A.L. Wang, H. Xu, J.X. Feng, L.X. Ding, Y.X. Tong, G.R. Li, J. Am. Chem. Soc. 135 (2013) 10703-10709.

[25] B. Duau, F.F. Ren, Y. Wang, C.Y. Zhai, C.Q. Wang, J. Guo, P. Yang, Y.K. Du, Chem. Asian J. 10 (2015) 667-673.

[26] Y. Wang, Y.Y. Shao, D.W. Matson, J.H. Li, Y.H. Lin, ACS Nano 4 (2010) 1790-1798.

[27] Y. Yang, W. Wang, Y.Q. Liu, F.X. Wang, D. Chai, Z.Q. Lei, Electrochim. Acta 154 (2015) 1-8.

[28] D.S. Geng, Y.H. Hu, Y.L. Li, R.Y. Li, X.L. Sun, Electrochem. Commun. 22 (2012) 65-68.

[29] H.J. Huang, H.Q. Chen, D.P. S un, X. Wang, J. Power Sources 204 (2012) 46-52.

[30] R.N. Singh, A. Singh, Anindita, Carbon 47 (2009) 271-278.

[31] W. Wang, Y. Yang, Y.Q. Liu, Z. Zhang, W.K. Dong, Z.Q. Lei, J. Power Sources 273 (2015) 631-637.

[32] Y.Z. Zhang, Y.E. Gu, S.X. Lin, J.P. Wei, Z.H. Wang, C.M. Wang, Y. Du, W. Ye, Electrochim. Acta 56 (2011) 8746-8751.

[33] Y.H. Qin, H.H. Yang, X.S. Zhang, P. Li, C.A. Ma, Int. J. Hydrogen Energy 35 (2010) 7667-7674.

[34] A. Brouzgou, L.L. Yan, S.Q. Song, Appl. Catal. B-Environ. 147 (2014) 481-489.

[35] T. Ramulifho, K.I. Ozoemena, R.M. Modibedi, C.J. Jafta, M.K. Mathe, Electrochim. Acta 59 (2012) 310-320.

[36] F. Kadirgan, S. Beyhan, T. Atilan, Int. J. Hydrogen Energy 34 (2009) 312-4320.

[37] H. Wang, R.F. Wang, H. Li, Q.F. Wang, J. Kang, Z.Q. Lei, Int. J. Hydrogen Energy 36 (2011) 839-848.

[38] M.L. Wang, W.W. Liu, C.D. Huang, Int. J. Hydrogen Energy 34 (2009) 2758-2764.

[39] S.L. Zhao, H.J. Yin, L. Du, G.P. Yin, Z.Y. Tang, S.Q. Liu, J. Mater. Chem. A 2 (2014) 3719-3724.

[40] B.M. Thamer, M.H. El-Newehy, N.A.M. Barakat, M.A. Abdelkareem, S.S. Al-Deyab, H.Y. Kim, Electrochim. Acta 142 (2014) 228-239.

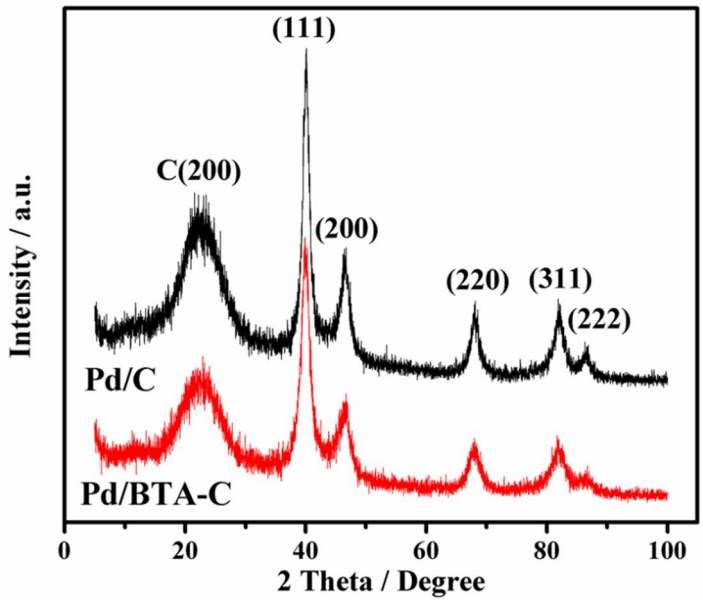

Fig. 1 XRD patterns of Pd/C and Pd/BTA-C.

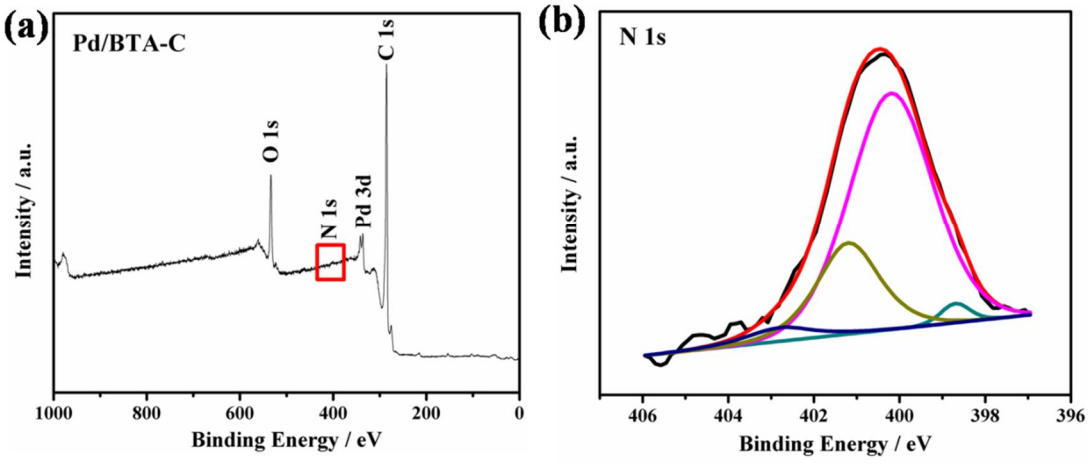

Fig. 2 The XPS (a) and N 1s XPS (b) spectra of Pd/BTA-C.

337

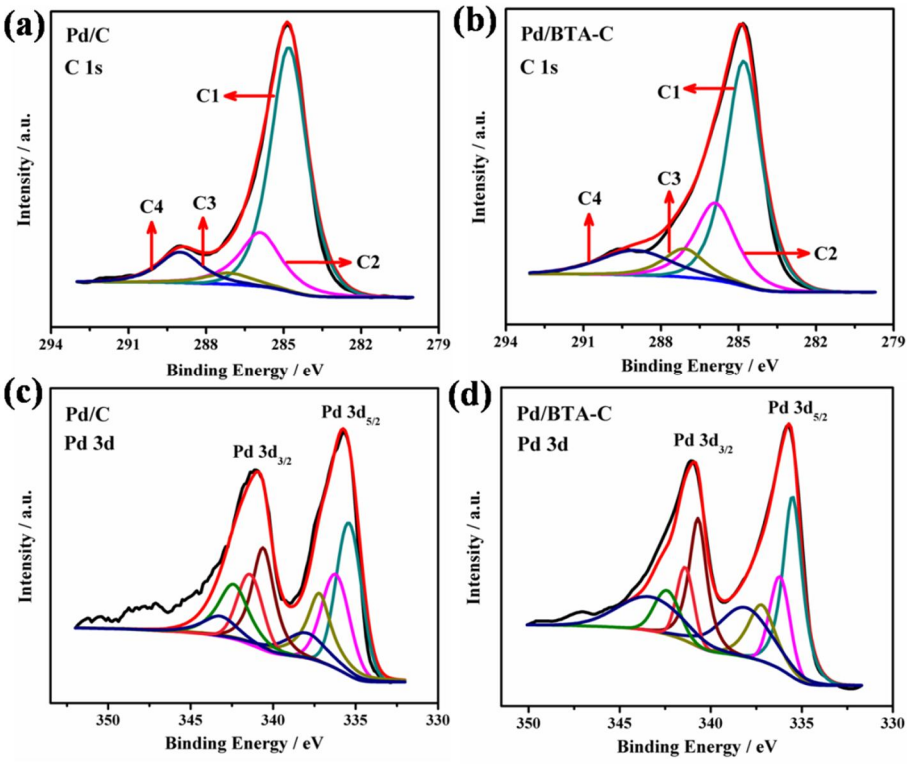

338

339 **Fig. 3** The C 1s XPS and Pd 3d spectra of Pd/C (a, c) and Pd/BTA-C (b, d).

340

341

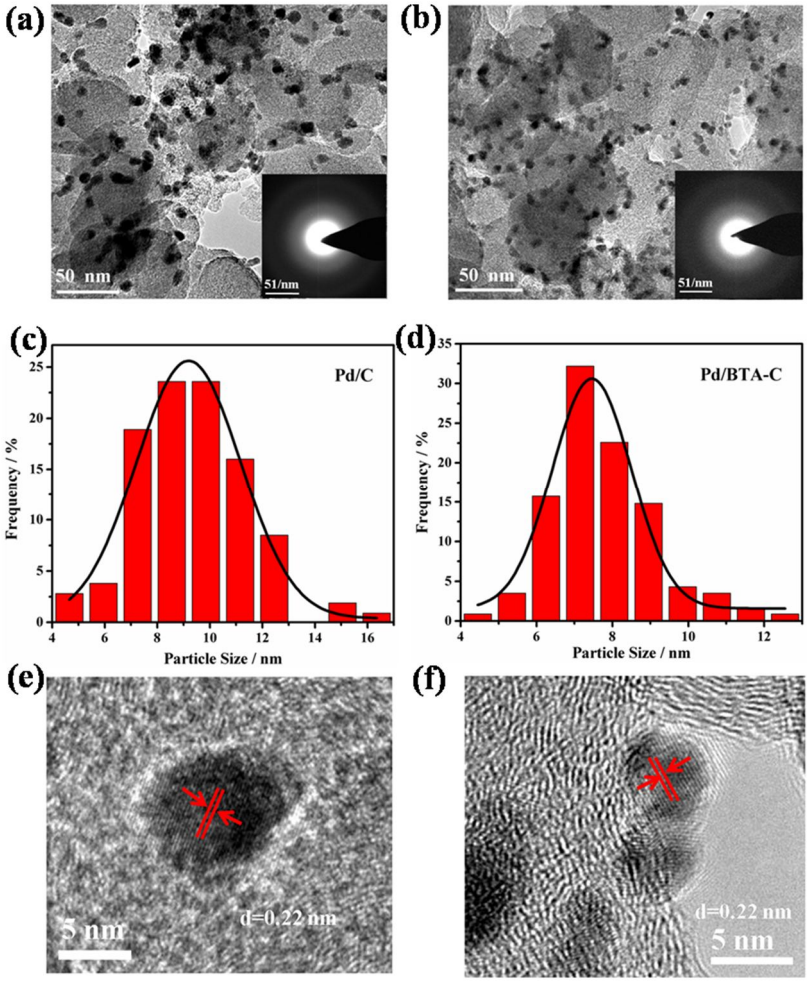

342

343 **Fig. 4** The TEM images, corresponded size distribution histograms and high resolution TEM

344 images of Pd/C (a, c, e) and Pd/BTA-C (b, d, f).

345

346

347

348

349

350

351

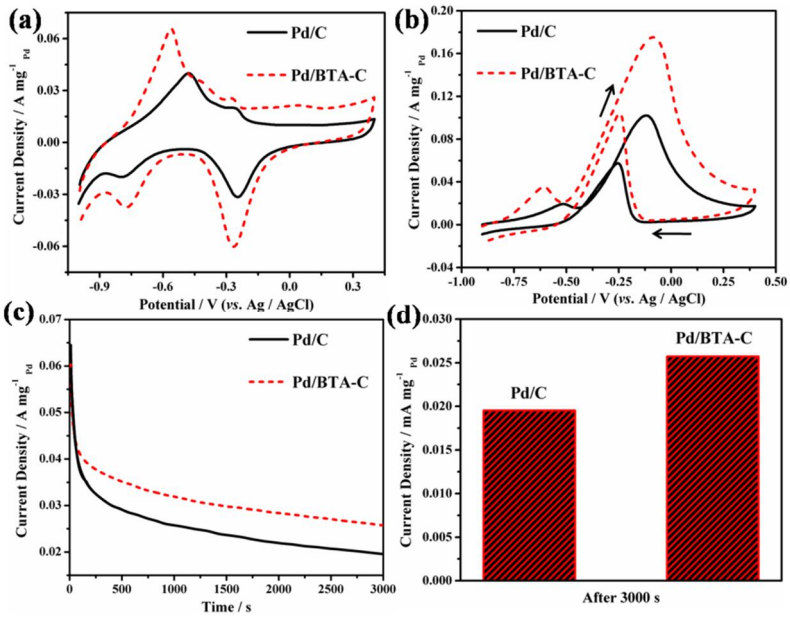

Fig. 5 Cyclic voltammetry of Pd/C and Pd/BTA-C in 0.1 M KOH solution (a) and in 0.1 M KOH + 0.5 M C_2H_5OH solution (b) saturated with N_2 at a scan rate of 50 mV s^{-1}. Chronoamperometric response of Pd/C and Pd/BTA-C (c) and the current density after 3000 s (d), fixed potential: -0.2 V (*vs.* Ag/AgCl).

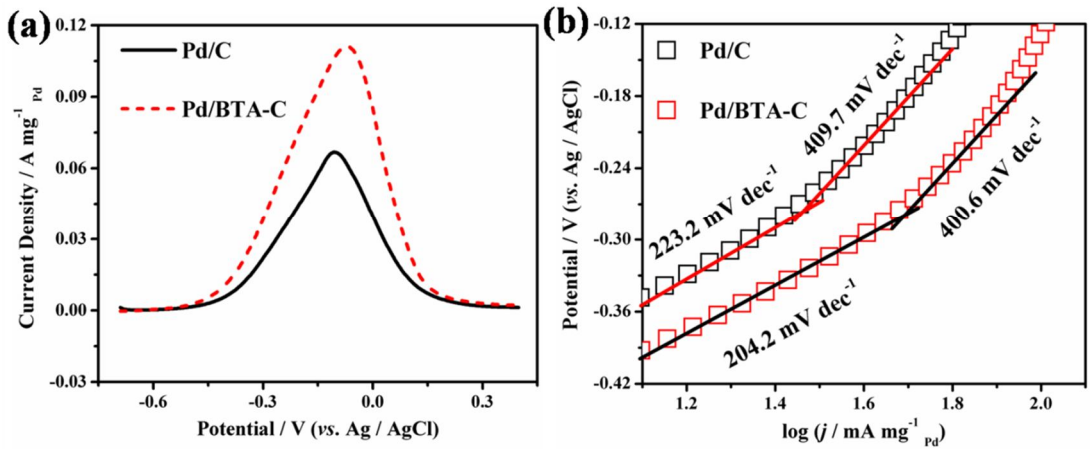

366

367 **Fig. 6** Linear sweep voltammetry of Pd/C and Pd/BTA-C in 0.1 M KOH + 0.5 M C_2H_5OH

368 solution saturated with N_2 at scan rate of 1 mV s^{-1} (a) and the corresponded Tafel plots (b).

369

370

371

372 **Tab. 1** Binding energy and relative intensities of C1s XPS spectra for Pd/C and

373 Pd/BTA-C catalysts.

C Species	C 1s Binding Energy (eV)	Peak Half Width (eV)	Relative Concentrations (%)
XPS C species of Pd/C			
C-C	284.8	1.67	67.2 %
C-OH	285.9	1.90	18.4 %
C-N	287.1	2.20	4.2 %
C-C=O	289.0	1.95	10.2 %
XPS C species of Pd/BTA-C			
C-C	284.8	1.63	56.5 %
C-OH	285.9	1.87	22.8 %
C-N	287.1	1.90	8.5 %
C-C=O	289.0	3.28	12.2 %

374

Tab. 2 Binding energy and relative intensities of Pd 3d XPS spectra for Pd/C and Pd/BTA-C catalysts.

Pd Species	Pd $3d_{5/2}$ Binding Energy (eV)	Peak Half Width (eV)	Relative Concentrations (%)
XPS Pd species of Pd/C			
Pd^0	335.4	1.80	38.4 %
$Pd(OH)_x$	336.2	2.00	26.4 %
PdO	337.2	1.72	23.5 %
PdO_2	338.0	3.00	11.7 %
XPS Pd species of Pd/BTA-C			
Pd^0	335.5	1.24	38.8 %
$Pd(OH)_x$	336.2	1.30	18.4 %
PdO	337.2	1.74	16.3 %
PdO_2	338.1	3.38	25.5 %

Electrocatalyst	Alcohol solution	EASA / cm^2 mg^{-1}	j_p / mA mg^{-1}_{Pd}	Ref
Pd/C	0.1 M KOH / 0.5 M C_2H_5OH	312.8	100	This work
Pd/BTA-C	0.1 M KOH / 0.5 M C_2H_5OH	583.0	180	This work

Tab. 3 Electrocatalytic properties of Pd catalysts loading on different supports for ethanol oxidation in alkaline media.

Pd/DMDAAC - RGO	1.0 M KOH / 1.0 M C_2H_5OH	1495	65 (mA cm^{-2})	[22]
Pd/PVP-graphene	1.0 M KOH / 0.5 M C_2H_5OH	231.5	439.8	[23]
Pd/PANI/Pd SNTAs	1.0 M KOH / 1.0 M C_2H_5OH	—	351.0	[24]

Note: EASA: The electrochemically active surface area; j_p: Forward peak current density; DMDAAC: Dimethyldiallylammonium chloride; PVP: polyvinylpyrrolidone; PANI: polyaniline; SNTA: sandwich-structured nanotube array.